A strontium isoscape of Italy for provenance studies

A strontium isoscape of Italy for provenance studies

Federico Lugli[1,2*], Anna Cipriani[2,3*], Luigi Bruno[2], Francesco Ronchetti[2], Claudio Cavazzuti[4,5], Stefano Benazzi[1,6]

1. Department of Cultural Heritage, University of Bologna, Via degli Ariani 1, 48121 Ravenna, Italy.
2. Department of Chemical and Geological Sciences, University of Modena and Reggio Emilia, 41125 Modena, Italy.
3. Lamont-Doherty Earth Observatory, Columbia University, Palisades, New York 10964, USA.
4. Dipartimento di Storia Culture Civiltà, University of Bologna, 40124 Bologna, Italia.
5. Department of Archaeology, Durham University, Durham, United Kingdom.
6. Max Planck Institute for Evolutionary Anthropology, Department of Human Evolution, 04103 Leipzig, Germany.

*corresponding authors: federico.lugli6@unibo.it; anna.cipriani@unimore.it

Abstract

We present a novel database of biological and geological $^{87}Sr/^{86}Sr$ values (n = 1920) from Italy, using literature data and newly analysed samples, for provenance purposes. We collected both bioavailable and non-bioavailable (i.e. rocks and bulk soils) data to attain a broader view of the Sr isotope variability of the Italian territory. These data were used to build isotope variability maps, namely isoscapes, through Kriging interpolations. We employed two different Kriging models, namely Ordinary Kriging and Universal Kriging, with a geolithological map of Italy categorized in isotope classes as external predictor. Model performances were evaluated through a 10-fold cross validation, yielding accurate $^{87}Sr/^{86}Sr$ predictions with root mean squared errors (RMSE) ranging between 0.0020 and 0.0024, dependent on the Kriging model and the sample class. Overall, the produced maps highlight a heterogeneous distribution of the $^{87}Sr/^{86}Sr$ across Italy, with the highest radiogenic values (>0.71) mainly localized in three areas, namely the Alps (Northern Italy), the Tuscany/Latium (Central Italy) and Calabria/Sicily (Southern Italy) magmatic/metamorphic terrains. The rest of the peninsula is characterized by values ranging between 0.707 and 0.710, mostly linked to sedimentary geological units of mixed nature. Finally, we took advantage of the case study of Fratta Polesine, to underscore the importance of choosing appropriate samples when building the local isoscape and of exploring different end-members when interpreting the local Sr isotope variability in mobility and provenance studies. Our user-friendly maps and database are freely accessible through the Geonode platform and will be updated over time to offer a state-of-the-art reference in mobility and provenance studies across the Italian landscape.

Keywords: $^{87}Sr/^{86}Sr$ ratio; Kriging; isotope map; spatial modelling; traceability.

1. Introduction

Geology is biological destiny: Whatever minerals land or are deposited in a place determine what or who can make a living there millions of years later.

(Dennis Overby 2021, New York Times)

Isoscape maps are built on isotope data and their creation is a process that embraces the application of isotope geochemistry to different facets of the geological sciences, including e.g., petrology, environmental geochemistry, pedology, sedimentology, biogeochemistry and hydrogeochemistry (Bataille et al., 2020). Understanding isotope distribution on the Earth surface benefits not only the geosciences but all those disciplines studying the provenance of foods, artifacts, animals and individuals.

Provenance is a central topic in archaeology, ecology, forensic science and even in social sciences and humanities. A broad range of methods from genetics to inorganic chemistry can be used to disentangle the geographical origin or the movement of goods/people across the landscape, depending on the nature of the material itself (see e.g. Gregoricka, 2021; Tommasini et al., 2018). Isotope fingerprinting is applied to a variety of samples (e.g. biological tissues, artifacts, rocks, waters) using various isotope systematics of elements such as oxygen (e.g. Pellegrini et al., 2016; Pederzani and Britton, 2019), hydrogen (e.g. Soto et al., 2013), lead (e.g. Vautour et al., 2015; Smith et al., 2019; Killick et al., 2020), strontium (e.g. Bentley, 2006), and sulphur (e.g. Bataille et al., 2021) targeting the different materials depending on the element abundance in the sample and the geobiological process under investigation. In this sense, the strontium $^{87}Sr/^{86}Sr$ ratio is an excellent tracer of low temperature terrestrial processes due to the abundance of elemental Sr and its mobility between the bio-, geo-, and hydro-spheres. While ^{87}Sr is the radiogenic-daughter of ^{87}Rb, ^{86}Sr is stable. Since both strontium and rubidium are ubiquitously present as trace elements within the Earth's crust, crustal rocks and mantle-derived materials will thus acquire different $^{87}Sr/^{86}Sr$ ratios in relation to their age and to their initial Sr and Rb contents (Faure and Mensing, 2005). Ultimately, this results in a high-variability of the $^{87}Sr/^{86}Sr$ across the landscape (see e.g. Voerkelius et al., 2010). From the bedrock, Sr is transferred to soil, where it mixes with different local pools as surface waters, groundwaters and atmospheric depositions (Bentley, 2006). This is also why 'bioavailable' Sr (i.e. biologically available) might

be isotopically different from the bedrock reservoir. In addition, the contribution of different minerals to the soil pool is variable due to e.g. differential weathering, Sr/Rb content and solubility (Sillen et al., 1998). For example, the contribution of Sr-rich carbonates to the local bioavailable reservoir is much larger than e.g. a more resistant to weathering Sr-rich silicate.

Sr ions exchanges at the Earth surface carry the isotopic fingerprint shaped over time by the radioactive decay of ^{87}Rb and transfer certain isotopes proportions from rocks to soils and waters. From the soil and water, Sr ions enter the ecosystem reaching plants, through root uptake, and animals, through food and drinking water (Capo et al., 1998). In vertebrates, Sr is then mainly fixed in the hydroxyapatite of tooth and bone tissues substituting calcium (Pors Nielsen, 2004). Across this pathway, mass-dependent Sr isotopic fractionation, as shown by e.g. the relative depletion of the stable $^{88}Sr/^{86}Sr$ ratio along the food chain, is likely to occur (Knudson et al., 2010). However, the fractionation of the $^{87}Sr/^{86}Sr$ ratio is deemed to be negligible and, anyhow, analytically corrected during mass spectrometry measurements as constant normalization to an internationally accepted ratio (Ehrlich et al., 2001).

Sr isotope data from biological samples of interest can be then compared with the local bioavailable Sr isotope ratio in order to understand whether the tissue formed locally or in a geologically different place, tracking the movements of people and goods through space and time (Ericson, 1985; Slovak and Paytan, 2012). Therefore, the subsequent step is to pin-point (more or less precisely) the specific geographic origin of the sample. In this sense, comparison with (inter)national geological maps can help to track the provenance of tissues formed on substrate whose isotopic ratio can be somehow predicted or expected, as for example in old metamorphic crystalline basements (i.e. highly radiogenic Sr isotope values) or depleted mantle-derived magmatic areas (low radiogenic Sr isotope values). Yet, a step-forward in isotope fingerprinting is the building of comparative isotopic maps that show the spatial distribution of the isotope signature (Bowen, 2010).

Using patchily-distributed measures of environmental samples, it is possible to build spatial models able to predict the local bioavailable $^{87}Sr/^{86}Sr$ ratio of a specific area. These data are then modelled through geostatistic tools in order to predict at best the $^{87}Sr/^{86}Sr$ ratio of areas with no available data. The resulting prediction maps are known as isoscapes (see Bataille et al., 2020). The utility of such implements has been demonstrated in several fields and they are today largely employed in provenance studies, as baselines for tracking the provenance of unknown specimens (e.g. Hobson et al., 2010; Muhlfeld et al., 2013; Song et al., 2014; Chesson et al., 2018; Colleter et al., 2021; Lazzerini et al., 2021). So far, national isoscapes have been produced for several European and extra-

European countries, employing and testing several different methods for the spatial interpolation, including machine learning (Montgomery et al., 2006; Evans et al., 2010; Frei and Frei, 2011; Bataille and Bowen, 2012; Pestle et al., 2013; Hartman and Richards, 2014; Copeland et al., 2016; Kookter et al., 2016; Laffoon et al., 2017; Bataille et al., 2018; Hedman et al., 2018; Willmes et al., 2018; Adams et al., 2019; Ladegaard-Pedersen et al., 2020; Scaffidi and Knudson, 2020; Snoeck et al., 2020; Wang et al., 2020; Frank et al., 2021; Funck et al., 2021; Washburnet al., 2021; Zieliński et al., 2021). Although a large amount of 'bioavailable' Sr data was produced in the past, mostly linked to food provenance and archaeological studies, a national isoscape for Italy is still lacking. A first attempt has been done by Emery et al. (2018), where an inverse distance weighting (IDW) interpolation was tested using some literature data to produce a preliminary Italian isoscape.

Here, we extended the database presented by Emery et al. (2018), using both novel and published data, and we performed a robust geospatial modelling, employing Ordinary Kriging and Universal Kriging (Willmes et al., 2018). Kriging is a widely used regression method in geostatistics and is based on the principle of 'spatial autocorrelation' (Krige, 1951). This consists in best-fitting a mathematical function (i.e. variogram) to a predetermined number of points with the aim of determining the output value for unknown locations and thus generating a continuous surface map (Oliver and Webster, 1990). We produced maps of Italy exploiting the Kriging methods and using an extensive dataset, which includes both 'bioavailable' and 'non-bioavailable' Sr isotope values (available at geochem.unimore.it/sr-isoscape-of-italy). The latter integrates bulk rock values from magmatic and metamorphic rocks. We acknowledge that to understand the provenance of biological samples, the best approach is to compare their isotopic fingerprint to bioavailable Sr isotope data. However, the inclusion of sparse rock values allowed us to understand the 'weight' of the bedrock influence on the local Sr isotope composition in specific areas of Italy. For this reason, we ultimately generated two maps, one with exclusively bioavailable data and one that includes all the values from the dataset. Maps are freely accessible at geochem.unimore.it/sr-isoscape-of-italy, through the GeoNode platform (geonode.org). $^{87}Sr/^{86}Sr$ data used to build the maps are also included in this publication as a supplementary spreadsheet.

2. Data and methods

2.1 Sample selection

Strontium isotope data were collected (n = 1831) from the literature (60 manuscripts) and categorized by source in six different clusters (Figure 1), namely 'plant', 'water', 'biomineral' (i.e. bones, teeth and bio-calcareous shells), 'food', 'soil' (including both exchangeable soil fractions and bulk soils) and 'rock' (mainly evaporites, metamorphic and magmatic rocks, and a few sedimentary bulk rocks). For each group, descriptive statistics analyses (i.e. mean, standard deviations and quantiles) were performed using Origin v. 2020 (data analysis and graphing software by OriginLab Corporation, Northampton, MA, USA) (see Table 1). We incorporated in our dataset both bioavailable and non-bioavailable (namely rocks and bulk soils) Sr isotope data and generated two maps (see below): one including the sole 'bioavailable' data and one including 'all' data ('bioavailable' + 'non-bioavailable'; see Table S1). This allowed us to obtain a broader overview of the Sr isotope distribution across Italy.

Table 1. Descriptive statistics for the different sample categories.

Category	N total	Mean	2 SD	Minimum	Median	Maximum	Interquartile Range (Q3 - Q1)
Plant	72	0.70881	0.00117	0.70778	0.70867	0.71122	0.00069
Water	476	0.71005	0.01013	0.70354	0.70887	0.76384	0.00120
Biomineral	471	0.70872	0.00182	0.70729	0.70866	0.71614	0.00094
Food	296	0.70926	0.00282	0.70679	0.70899	0.72071	0.00071
Soil	273	0.70994	0.00549	0.70528	0.7091	0.72379	0.00131
Rock	332	0.71064	0.01081	0.70319	0.70898	0.753	0.00212
Whole dataset ('all')	1920	0.70964	0.00734	0.70319	0.70888	0.76384	0.00105

Novel data (n = 89) were generated from modern environmental and archaeological samples by solution MC-ICPMS analyses. Samples include modern vegetation, archaeological and modern teeth, snails, waters, rocks and soils. These samples are from areas where archaeological studies are in progress and thus were integrated into the database. Five meteoric water samples collected from pluviometers located in the Emilian Apennine (Montecagno, 44°19'57.76'' N; 10°21'58.57'' E) were also measured for their Sr isotopic composition. These values were not included in the spatial model, but are presented as possible end-members for the Sr cycle in the biosphere, possibly helpful for future studies on Sr mixing (Table 2).

Table 2. Sr isotopes of meteoric waters measured in this study.

Latitude	Longitude	Sampling date	Material	$^{87}Sr/^{86}Sr$	2 SE
44°19'57.76'' N	10°21'58.57'' E	March 2016	Meteoric water	0.70848	0.00001
44°19'57.76'' N	10°21'58.57'' E	June 2016	Meteoric water	0.70873	0.00001
44°19'57.76'' N	10°21'58.57'' E	October 2016	Meteoric water	0.70882	0.00001
44°19'57.76'' N	10°21'58.57'' E	March 2017	Meteoric water	0.70924	0.00001
44°19'57.76'' N	10°21'58.57'' E	July 2017	Meteoric water	0.70897	0.00001

2.2. Solution MC-ICPMS

Samples were processed at the Geochemistry Lab of the Department of Chemical and Geological Sciences (University of Modena and Reggio Emilia). All the reagents employed were of suprapur grade. Biominerals (i.e. teeth and snail shells) were cleaned with MilliQ water and digested using concentrated HNO_3. The bioavailable Sr fraction from soils instead was extracted using 0.25M acetic acid. Bulk rocks samples were totally digested using a mixture of concentrated HNO_3 and HF. Waters were filtered (5 μm) and acidified with HNO_3 to a concentration of 3M. After drying and re-dissolution by 3M HNO_3, all samples were processed using the Eichrom Sr-spec resin. The $^{87}Sr/^{86}Sr$ ratios were determined by Neptune MC-ICPMS, housed at the Centro Interdipartimentale Grandi Strumenti of the University of Modena and Reggio Emilia. Detailed protocols are described in Lugli et al. (2017, 2018) and Argentino et al. (2021). Repeated measures of NBS987 yielded an $^{87}Sr/^{86}Sr$ value of 0.710237 ± 0.000011 (2 SD; n = 18). All values were normalized to an NBS987 accepted value of 0.710248 (McArthur et al., 2001).

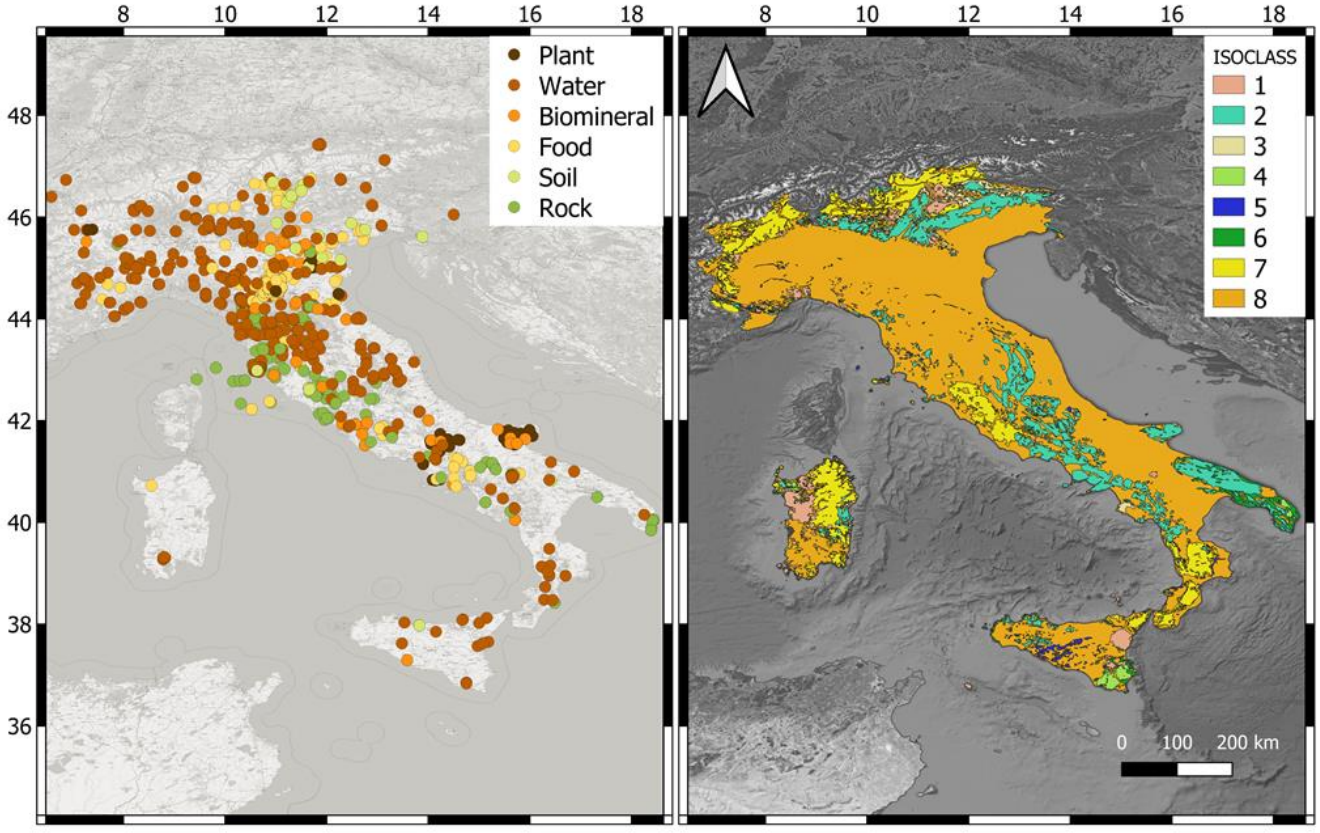

Figure 1. Left panel: locations of the data points considered in this study. Most of the data are from literature, with the addition of novel unpublished environmental/archaeological samples. All the samples in the 'plant', 'water', 'biomineral' and 'food' categories are considered 'bioavailable', in addition to 'soil' leachates. 'Rock' and bulk 'soil' are considered 'non-

bioavailable'. This map was built in QGIS 3.18.1 (QGIS Development Team 2021, QGIS Geographic Information System. Open Source Geospatial Foundation Project. http://qgis.osgeo.org), exploiting the OpenStreetMap service. Right panel: Isoclass map of Italy that is a map of the Italian geolithologies classified according to their expected isotope values. This map is based on the geolithological map of Italy available at the Geoportale Nazionale (http://wms.pcn.minambiente.it/ogc?map=/ms_ogc/wfs/Carta_geolitologica.map); the satellite map is provided by Google through the QGIS QuickMapServices plug-in. Isoclass 1: plutonic and volcanic rocks related to MORB mantle magmatism of different ages. Isoclass 2: marine carbonate rock formations of Late Triassic, Cretaceous and Jurassic ages. Isoclass 3: Early and Middle Triassic and Paleogenic marine carbonate rocks. Isoclass 4: Early and Medium Miocene marine carbonate formations. Isoclass 5: Late Miocene carbonates. Isoclass 6: Pleistocene and Pliocene carbonate formations. Isoclass 7: old metamorphic and magmatic rocks of the crystalline basement and younger volcanics whose magmatism is affected by a radiogenic Sr isotope source. Isoclass 8: all the geolithologies not attributed to an isotope class due to their hybrid nature (i.e. siliciclastic rocks) or to their large Sr isotope variability (i.e., Permian to Devonian carbonates have a very wide range of Sr isotope ratios across several of our defined classes).

2.3 Geospatial modelling

All the identified literature data and new data were grouped in an Excel worksheet and imported into SAGA 7.9 for geospatial modelling (Conrad et al., 2015). We employed two different models to obtain the interpolated $^{87}Sr/^{86}Sr$ maps, namely Ordinary Kriging and Universal Kriging. The latter is drifted using a geological map of Italy as auxiliary predictor, similarly to the Kriging model with external drift of Willmes et al. (2018). However, unlike Willmes et al. (2018), where the isotope groups were defined using clustering techniques on the data itself, we relied on a simplified geological map of Italy (Figure 1), generated *ad hoc* for this project, combining geolithologies and expected isotope values of the rock formations (see Figure S1 and the Supplementary text 'Geological Setting'). In particular, we defined eight isotope classes ('isoclass', Figure 1) taking advantage of: 1) the expected Sr isotope range of certain rock formations outcropping in the Italian peninsula as reported in the literature; 2) the categorization of geological units (i.e. metamorphic, magmatic, sedimentary, etc.) of the Italian geolithological map (published by the Geoportale Nazionale, pcn.minambiente.it; see also Figure S1); 3) the Sr isotope seawater curve of McArthur et al (2001), which in Italy finds wide application due to the continuous marine carbonate deposits from the Triassic to the Neogene preserved across the peninsula. Notably a relatively high number of isotope data is available in the literature for metamorphic and magmatic rocks across Italy, which have been measured to understand the geodynamic events that led to the formation of the Alps and Apennines

and their emplacement at crustal level. Although most of these data were not included in the database, because no geolocalization was available, their isotope signature was used to define isoclasses as building blocks of the Italian Sr isomap. In addition, several published Sr isotope data were measured on single mineral phases and therefore, being not always representative of the bulk rock, could not be used for our purpose.

The range of Sr isotope values of the eight isoclasses is defined as follows: Isoclass 1 (expected $^{87}Sr/^{86}Sr < 0.70682$) includes plutonic and volcanic rocks related to MORB mantle magmatism of different ages. Isoclass 2 ($0.70682 <$ expected $^{87}Sr/^{86}Sr < 0.70783$) includes mainly marine carbonate rock formations of Late Triassic, Cretaceous and Jurassic ages. Isoclass 3 ($0.70783 <$ expected $^{87}Sr/^{86}Sr < 0.70825$) includes Early and Middle Triassic and Paleogenic marine carbonate rocks. Isoclass 4 ($0.70825 <$ expected $^{87}Sr/^{86}Sr < 0.70885$) includes Early and Medium Miocene marine carbonate formations. Isoclass 5 ($0.70885 <$ expected $^{87}Sr/^{86}Sr < 0.70903$) includes mainly Late Miocene carbonates. Isoclass 6 ($0.70903 <$ expected $^{87}Sr/^{86}Sr < 0.70920$) includes Pleistocene and Pliocene carbonate formations. Isoclass 7 (expected $^{87}Sr/^{86}Sr > 0.70920$) includes old metamorphic and magmatic rocks of the crystalline basement and younger volcanics whose magmatism is affected by a radiogenic Sr isotope source. Isoclass 8 finally includes all the geolithologies that we were not able to attribute to an isotope class due to their hybrid nature (i.e. siliciclastic rocks) or to their wide Sr isotope variability (i.e., Permian to Devonian carbonates have a very wide range of Sr isotope ratios across several of our defined classes).

In attributing the isoclass to a particular geolithology or formation we confronted local rock values from literature and, whenever possible, double checked their consistency with the bioavailable values of our database. When no data were available, we considered the type of rock (i.e. mineralogy) and the age of formation. Initially, we defined several more isoclasses in the Sr isotope range especially in the range between 0.7092 and very radiogenic values (up to 0.75). However, we could attribute with certainty only a few data points from Sardinia to these classes, and therefore we finally grouped all Sr isotope ratios > 0.7092 in a unique class (isoclass 7). We stress that the attribution of an isoclass has not been arbitrary and any attribution is either backed up by isotopic data or consistent with a particular type of magmatism or deposition event (i.e. seawater curve for marine carbonates of McArthur et al., 2001).

For geospatial modelling, the observed variograms were fit through a linear model, with a searching range of ca. 180 km. As in Hoogewerff et al. (2019), the semivariograms obtained here showed a cyclical-like structure, with a first maximum located at approximately 250 km (Figure S2). The prediction power of the models was evaluated using a 10-fold cross-validation method through SAGA 7.9. The interpolated Kriging models were imported into

QGIS 3.18 (QGIS Development Team 2021, QGIS Geographic Information System. Open Source Geospatial Foundation Project. http://qgis.osgeo.org) to generate the final distribution maps (freely available online at geochem.unimore.it/sr-isoscape-of-italy). We note here that Sardinia was excluded from the Ordinary Kriging due to the low number of data from the area.

3. Results and discussion

3.1. Data description and distribution

Descriptive statistics for the data considered in this study are reported in Tables 1 and S1 and summarized in Figures 2 and S3. When categorized, the 'rock' group has as expected the larger variance of the whole dataset, with an $^{87}Sr/^{86}Sr$ ranging from 0.70319 to 0.75300 (Figure 2). This group also shows the averagely highest Sr isotope values (0.7106). On the contrary, plants and biominerals are characterized on average by the lowest Sr isotope values (0.7087-0.7088). The most extreme values of the dataset are found within 'rock' (0.70319) and 'water' (0.76384) groups (see Table 1). Bioavailable samples show an average $^{87}Sr/^{86}Sr$ ratio of 0.70941 ± 0.00632 (2 SD), and span between 0.70354 and 0.76384, with a median value of 0.70883. The kernel density distribution of the bioavailable data is strongly asymmetric and leptokurtic (skewness = 8.14; kurtosis = 99.16). Notably, the non-bioavailable samples, including all the rocks and bulk soils, display an average $^{87}Sr/^{86}Sr$ ratio of 0.71069 ± 0.01054 (2 SD), ranging between 0.70319 and 0.75300, with a median value of 0.70900 (Table S1). The distribution of the non-bioavailable dataset is asymmetric but less leptokurtic than the bioavailable (skewness = 3.93; kurtosis = 22.40). Yet, we stress that the number of non-bioavailable data (n = 352) here considered is remarkably lower than the data in the bioavailable dataset (n = 1568), potentially influencing our observations on the data. Similarly, the uneven spatial distribution of 'non-bioavailable' samples across Italy certainly influenced data evaluations and use for this class. $^{87}Sr/^{86}Sr$ ratios of the bioavailable samples were also exploratively plotted against latitude and longitude (Figure 3), searching for potential correlations between these variables. However, no statistically significant trend was observed (both $R^2 < 0.1$). Yet, the two graphs clearly show a preferential distribution of the highest radiogenic Sr values northwards (latitude 44-47° N) and eastwards (longitude 7-12° E). This is expected due to the presence of old metamorphic and magmatic rocks in the Alpine area and magmatic-metamorphic provinces in Central Italy (Tuscany, Latium), and also evident when data are plotted by Italian macroregions (Figure 2).

Five meteoric waters, not included in the previous statistics evaluations (and the interpolated maps) range between 0.70848 and 0.70924, and represent an end-member of the Sr bioavailable cycle. These five waters were sampled from the same pluviometer located in the Emilian Apennine, and they were seasonally collected ca. 3-to-5 months apart from each other. These data highlight a remarkable temporal variability of the local rainwater likely due to the changing contribution of seawater aerosol and crustal dust, with a possible important influence on the local bioavailable Sr (Négrel et al., 2007).

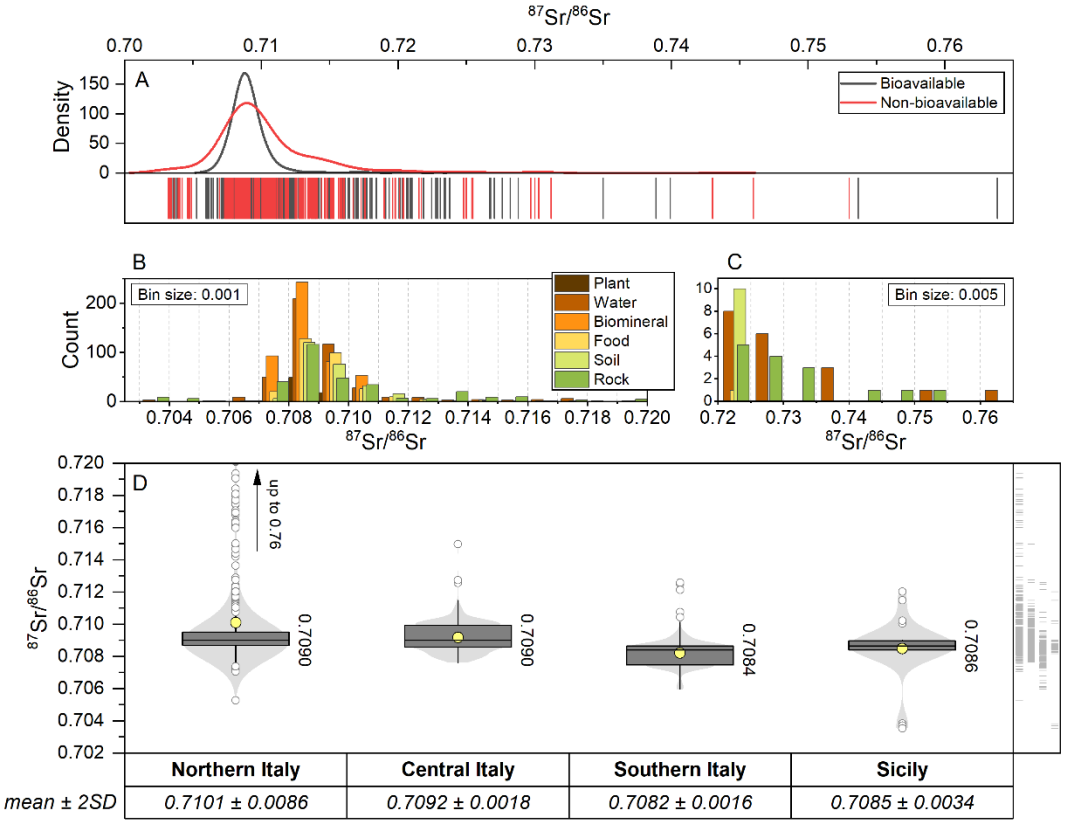

Figure 2. Data exploration. A) Kernel density estimation of bioavailable (n = 1568) vs. non-bioavailable (n = 352) $^{87}Sr/^{86}Sr$ data. B) Superimposed histogram representing the different sample categories between 0.702 and 0.720, with a bin size of 0.001. C) Superimposed histogram of the different sample categories between 0.720 and 0.77, with a bin size of 0.005. Note that the y-scale ranges of the histograms ('count') are different. D) Bioavailable Sr isotope data grouped by geographical areas (macroregions) of Italy, defined according to the National Institute of Statistics (istat.it); median values are labelled close to the box plots; average values ± 2 SD are also reported.

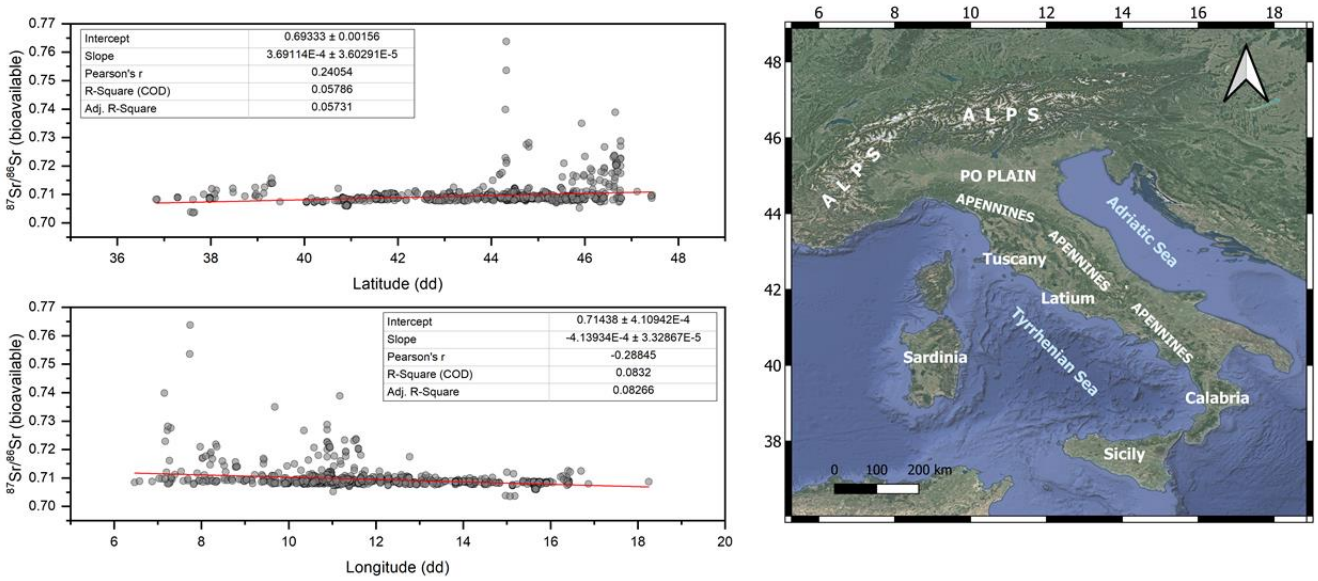

Figure 3. The $^{87}Sr/^{86}Sr$ ratios plotted against latitude and longitude (decimal degrees). No significant linear trend appears; however, most of the radiogenic Sr data are latitudinally distributed northwards and longitudinally eastwards. Graphs and linear trends were produced using Origin v. 2020. Right panel: a geographic map of Italy is reported as reference; the main areas cited in the manuscript are labelled.

3.2. Maps

The isoclass map of Italy (Figure 1) allows a first order distinction between the radiogenic Sr isotope provinces, related to the 'old' crustal and radiogenic Sr isotope magmatism units mainly present in the Alps, Calabria, Sardinia and Central Italy, and the unradiogenic provinces related to the depleted mantle magmatism mainly in the Southern Alps and Sicily. Yet, more information can be gathered through the isoscape maps (Figures 4 and 5). These were built modelling the two datasets, namely 'bioavailable' and 'all'. Each figure includes two maps obtained with two distinct Kriging approaches: Ordinary and Universal with external drift. The evaluation of performance of the two models is reported in Table 3. Both methods produced satisfying results, with relatively low normalized root mean squared errors (NRMSE ~3-4%), explaining between ~60 and ~70% of the isoscape variance (R^2). In general, Universal Kriging (with eternal drift) seems to outperform Ordinary Kriging, although the difference is not remarkable (Table 3). The lowest RMSE is observed for the 'bioavailable' Universal Kriging, and is equal to 0.0020; instead, the highest RMSE (0.0024) was obtained for the 'all' Ordinary Kriging model. Altogether, the presence of non-bioavailable (un)radiogenic end-members in the 'all' database seems to limit the prediction power of the Kriging method, both in terms of data over-fitting (higher R^2) and worse variogram

modelling (see also Figure S4). To further evaluate the prediction of our modelling we measured the prediction standard errors for the Kriging maps (Figure S4). Both models (i.e. Ordinary and Universal) show similar standard prediction errors, ranging from ca. 5E-7 to 5E-6 for the 'bioavailable' dataset and from 2E-7 to 2E-5 for the 'all' dataset. These errors are low when compared with other spatial interpolation presented in literature for isoscapes (e.g. Willmes et al., 2018; Adams et al., 2019; Wang et al., 2020). Such low values are possibly related to the high number of samples considered in this study (total n = 1920), evenly distributed across Italy (see Figure 1), compared to the available literature studies. Largest errors indeed can be found in Sicily and Sardinia, where the number of samples is significantly lower than in other areas (Figure S4).

Table 3. 10-fold cross validation results for Kiriging model performances trough SAGA 7.9.

Model	Dataset	N. data points	RMSE	Normalized RMSE (%)	R^2 (%)
Ordinary Kiring	'bioavailable'	1568	0.0021	3.5	59.5
	'all'	1920	0.0024	3.9	66.0
Universal Kiring	'bioavailable'	1568	0.0020	3.4	59.0
	'all'	1920	0.0022	3.6	69.7

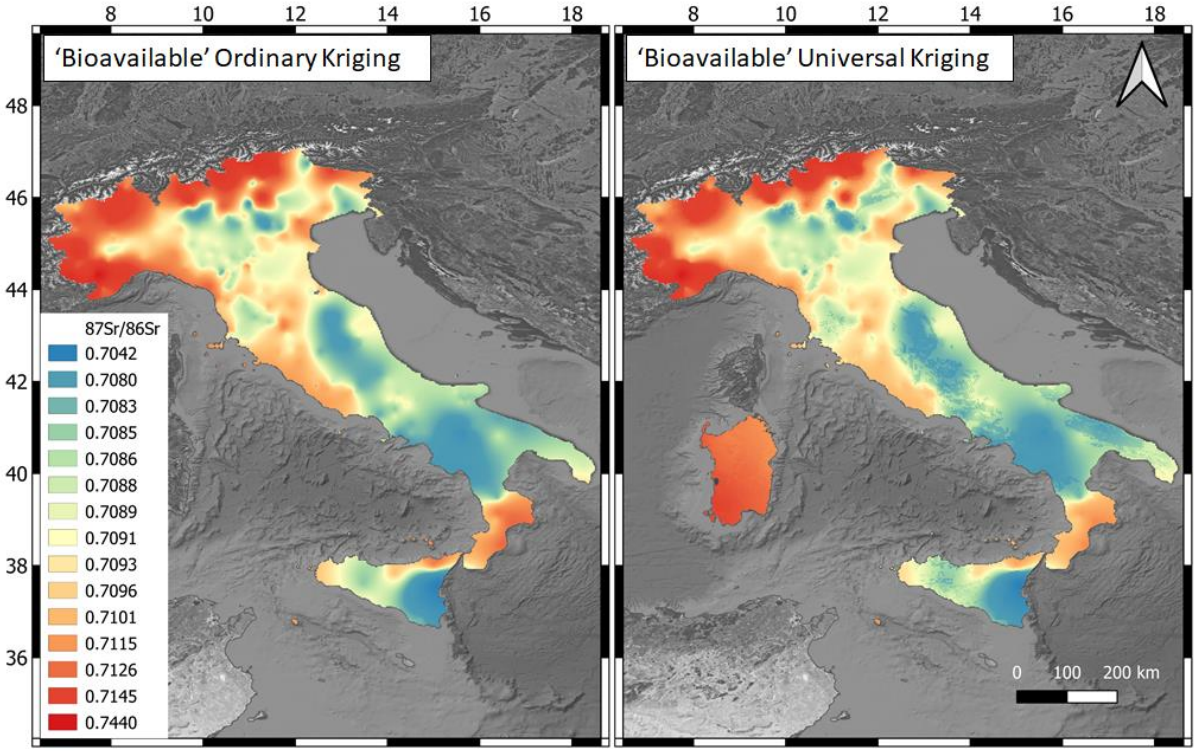

Figure 4. Ordinary and Universal (with external drift) kriging models obtained for the 'bioavailable' $^{87}Sr/^{86}Sr$ dataset. Maps were obtained using SAGA 7.9 and QGIS 3.8.

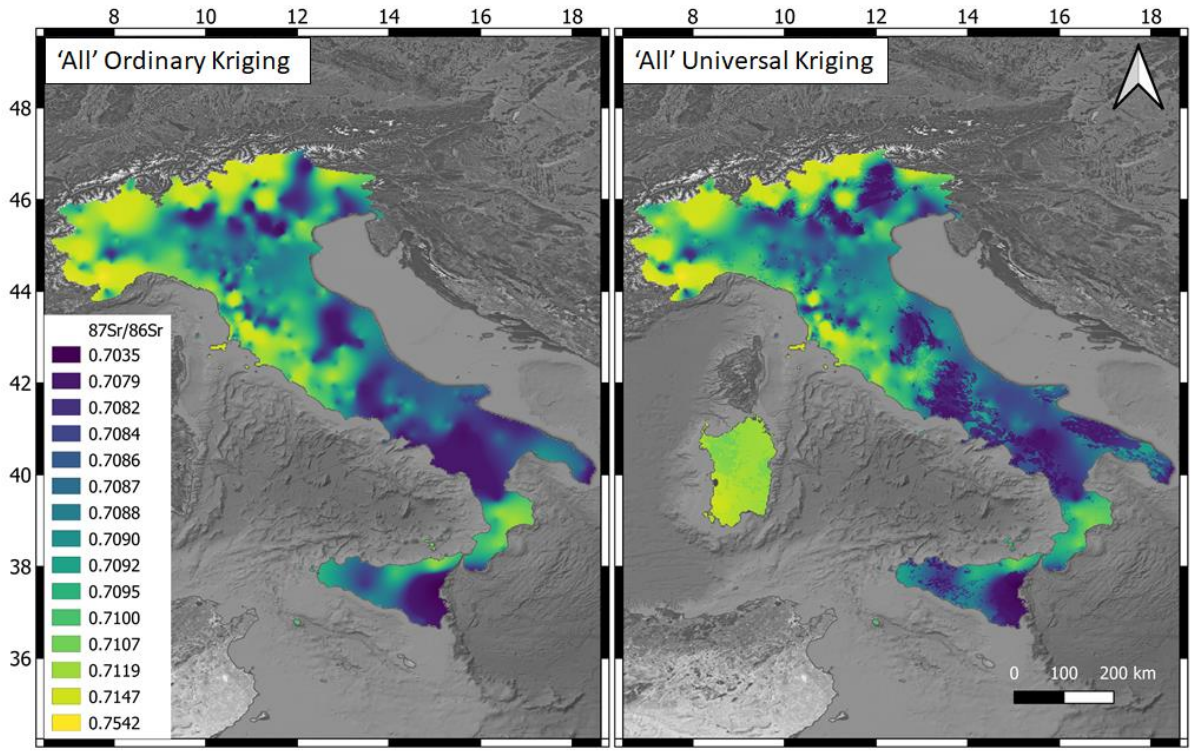

Figure 5. Ordinary and Universal (with external drift) kriging models obtained for the 'all' $^{87}Sr/^{86}Sr$ dataset. Maps were obtained using SAGA 7.9 and QGIS 3.8.

The 'bioavailable' (Figure 4) and the 'all' (Figure 5) maps show similar spatial distribution of the $^{87}Sr/^{86}Sr$ ratios, with the highest radiogenic values clustered in well-defined geological areas of Italy, namely the Alps, the Tuscan Magmatic Province, the Latium volcanic area and the Calabria crystalline basement (Southern Italy). These values are of course related to the radiogenic nature of the natural components from these areas included in our database. Contrariwise, low Sr isotope values are generally present in areas characterized by depleted mantle magmatism such as in Sicily and in Campania and where old carbonates (older than Pliocene) outcrop.

The largest differences in terms of isoscape predicted values among the 'all' and the 'bioavailable' maps arise indeed in these areas (particularly Tuscany and Latium), due to the presence of even higher radiogenic values in local rocks, only partially identified in the bioavailable pool (see Figure S5). The north-western Alpine area also shows significant differences (both in negative and positive) between the two datasets. However, here, only few rock values are present within the 'all' database. This suggests that the observed variations (see e.g. Cuneo area, north-

western Italy) are probably linked to model's predictions inaccuracies rather than actual variations of the $^{87}Sr/^{86}Sr$ ratio.

Overall, several small 'hotspots' (both negative and positive) can be recognized when comparing the predictions of the two datasets, particularly in the Alps. We stress that the number of samples in these areas is lower than in other localities; however, another explanation might lie in the complex geometry of the Alps where the bioavailable Sr isotope ratios might differ from those of the exposed rocks because of the geological complexity of the nappes that overthrust each other in the belt and therefore in the differential contributions to the bioavailable Sr possibly from other reservoirs.

Sharper details of the isotope zones can be observed in the Universal Kriging map compared to the Ordinary Kriging, due to the definite isoclass boundaries of the guiding map. In general, when looking at specific areas of the map, the Universal Kriging model should be more accurate in terms of spatial prediction, particularly for those areas with few data available. However, the Ordinary Kriging map seems to better mimic the natural averaging of Sr isotope values due to weathering and mixing processes.

3.3. Definition of the local bioavailable Sr baseline for human provenance: a case study

Defining the local bioavailable Sr baseline is currently a hot topic in archaeology and anthropology. Common methods include the measurement of modern environmental samples as waters, plants, snail shells and soil leachates (Bentley, 2006; Maurer et al., 2012; Ladegaard-Pedersen et al., 2020; Toncala et al., 2020), but also through the analysis of local (archaeological) fauna (see e.g. Lugli et al., 2019). Some studies also showed the power of using statistical methods to detect outliers (as Tukey's fences and median absolute deviations) among the human's skeletal isotopic dataset, to constrain local vs. non-local individuals (Lightfoot and O'Connell, 2016; Cavazzuti et al., 2021). Once defined, the local baseline is then used to comprehend the mobility patterns of the investigated human population (i.e. autochthonous vs. allochthonous individuals). However, there is no general consensus on the best practices to employ for determining the local Sr baseline (e.g. Maurer et al., 2012; Britton et al., 2020; Weber et al., 2021). All the methods have indeed intrinsic flaws linked to various sources of error such as anthropogenic contaminations on environmental samples (Thomsen and Andreasen, 2019), temporal changes in the Sr mixing end-members (e.g. Erel and Torrent, 2010; Han et al., 2019) or simply erroneous *a priori* assumptions. For example, were 'local' animals actually 'local'? What is their real home range? Are modern plants,

growing on modern soils, isotopically representative of the ancient landscape? All these are open questions that call for further investigations and can lead to data misinterpretation if not considered.

We take advantage of some of the novel data measured for this study to further discuss this issue, focusing on the Bronze Age archaeological site of Fratta Polesine (Cardarelli et al., 2015; Cavazzuti et al., 2019a) in the Po plain (Northern Italy, see also Cavazzuti et al., 2019b). Locally, the geology is characterized by Holocene alluvial debris, mainly composed of siliciclastic sedimentary deposits related to the erosion of the Alpine belt. To test the robusticity of isoscape predictions, we built a bioavailable Sr isoscape excluding the bioavailable data from the site (n=12), to compare Ordinary Kriging interpolated data against the Fratta Polesine measured dataset (Figure 6). The Ordinary Kriging interpolated $^{87}Sr/^{86}Sr$ ratio, in a radius of 10 km from the site, ranges between 0.7091 and 0.7096, with a median value of 0.7094. The measured bioavailable data from Fratta Polesine are averagely less radiogenic (0.7089) but more variable, ranging between 0.7085 (snail) and 0.7094 (modern shallow rooted plant). These specimens plot as three distinct clusters, with plant and soils showing the highest values (0.7092-0.7094), snails the lowest (0.7085-0.7086), and animal enamel falling in the middle (0.7088-0.7089). Such variability in our measured data suggests that different end-members influenced in different ways the environmental specimens. Plants (mostly shallow rooted plants) and soils are indeed likely to be more influenced by atmospheric deposition and anthropogenic contaminants. Yet, the rainwaters from the Apennines show a maximum value of 0.7092 (Table 2), suggesting that other sources (as dust, fertilizers and/or other antropic sources) might have contributed to the plant-soil pool at Fratta Polesine (Thomsen and Andreasen, 2019). Our isoscape agrees with the presence of higher radiogenic values towards the north-east. Hence, we can alternatively hypothesize that underground waters flowing southwards from the Alps into the Po plain might have influenced the local isotope fingerprint of soils and plants from Fratta Polesine.

Snail shells are characterized by the lowest radiogenic $^{87}Sr/^{86}Sr$ ratios among the measured samples. Previous studies linked this fact to the amount of soil carbonate incorporated into the diet of land snails (Yanes et al., 2008; Maurer et al., 2012; Britton et al., 2020), suggesting that $^{87}Sr/^{86}Sr$ are commonly shifted towards local carbonates values. In addition, Evans et al. (2010) found that the $^{87}Sr/^{86}Sr$ ratio of snail shells can be biased by the Sr of local meteoric water. We have no data of rainwaters from Fratta Polesine, however data from the Apennines show on average slightly higher $^{87}Sr/^{86}Sr$ ratios than snails. Yet, the large isotopic variability showed by our meteoric waters and the distance (ca. 130 km) between the sampling site and Fratta Polesine make it difficult to draw accurate assumptions. Altogether, such evidence indicates that snail data need to be interpreted with cautions when

extrapolating the local Sr bioavailable signature, being possibly different from local mammal's $^{87}Sr/^{86}Sr$ ratios. Fratta Polesine mammals' enamel shows indeed intermediate values (0.7088-0.7090), possibly reflecting different sources of drinking water and food (Toncala et al., 2020). For example, the (domesticated?) dog and pig teeth are isotopically compatible with the Po river water, one of the main sources of drinking water close to Fratta Polesine. Human data presented in Cavazzuti et al. (2019a) show a median $^{87}Sr/^{86}Sr$ ratio of 0.7089, with an interquartile range (Q3-Q1) of 0.0006, indicating that most of the individuals are compatible with the baseline of the site and few plot outside the local environmental variability (see Cavazzuti et al., 2019a for more details).

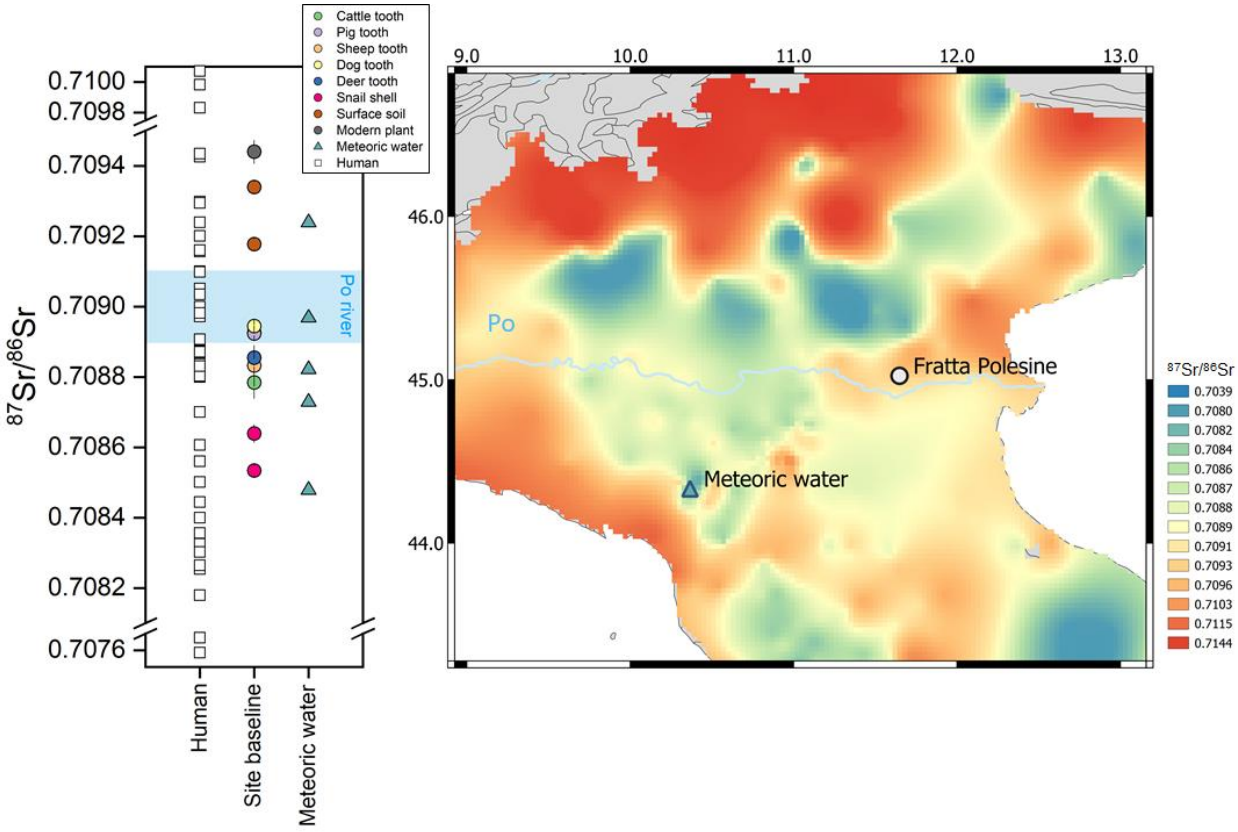

Figure 6. Local baseline at the Bronze Age site of Fratta Polesine (Rovigo, Veneto). Analysed samples include animal tooth enamel, snail shells, surface soil leachates and vegetation. Human data (including both enamel and cremated petrous bone specimens) are from Cavazzuti et al. (2019a). In the graph, meteoric water data from the Apennines (blue triangles) and water data (light blue area) from the Po river (sampling locations close to the site) are reported for comparison. The Sr bioavailable map on the right panel is an Ordinary Kriging interpolation, without the local data from Fratta Polesine. The local (<10 km) predicted $^{87}Sr/^{86}Sr$ range at the site is 0.7091-0.7096 (median 0.7094). The Po river is also shown on the map.

Overall, these data suggest that soils (leachates) and plants best reflect the local bioavailable Sr pool, although possibly contaminated by modern and/or anthropic end-members. Fauna enamel, if truly local as in the case of domesticated macro-mammals or small home range micro-mammals, mixes various bioavailable Sr sources and more closely mimics the local food and drinking sources. Such evidence clearly highlights the intrinsic limits in using isoscapes, which are commonly composed by a patchwork of literature data from different samples, or modelled on specific samples collected *ad hoc* (as soils or plants). Yet, we stress here that Sr isotopes need to be interpreted following an 'exclusion' principle, and thus employed to *discard* possible areas as point of origin (Holt et al., 2021). This, in turn, suggests that provenancing through Sr isoscapes, and isotope baselines in general, need to be performed with caution. Hence, Sr isoscapes must be considered as 'guides' for data interpretation, rather than an unequivocal provenancing tool, justifying their composite nature to better understand the variability of local Sr pools.

4. Conclusions

Benefiting from the large availability of Sr isotope data in the literature, we collected a large amount of georeferenced Sr isotope values specifically for Italy. Owing to this database, we were able to produce $^{87}Sr/^{86}Sr$ prediction maps by geostatistical modelling, namely Ordinary Kriging and Universal Kriging. Model performances were evaluated through 10-fold cross validations, resulting in RMSE ranging between 0.0020 and 0.0024.

Bioavailable Sr isotope values across Italy show a remarkable variability, with the Alps and certain metamorphic/magmatic terrains displaying the highest radiogenic values, and are in general well-consistent with the underlying bedrock type.

We took advantage of the generated database to discuss a local case study (Fratta Polesine) and the definition of local baseline in archaeological studies, a currently hot-topic within the field of provenance and mobility studies. Specifically, we built a regional isoscape, excluding local data from Fratta Polesine, to test the robusticity of the spatial interpolation. We found that the human median value and the local measured samples, although presenting a larger isotopic variability, fit the isoscape-predicted $^{87}Sr/^{86}Sr$ local range. Hence, regional and (extra)national isoscapes are key in understanding the local Sr pool, broadening our understanding on the mixing of the different end-members to obtain certain isotope signatures in (geo)biological samples.

Distribution maps of Sr isotopes provide a solid interpretative basis for provenance and traceability studies. They build upon isotope data from different types of biological and geological samples, including water and represent a synthesis of the outer workings of the Earth system and of the long term evolution of the Sr isotope system. Our maps and database are freely accessible online and will be updated in the future when new data become available. In this sense, we will continue to collect and analyse new environmental samples from low-density areas (such as Sicily and Sardinia) to improve the prediction power of the models. In addition, we plan to employ novel methods for the spatial modelling of isotope data, using different predictors and machine learning approaches.

Acknowledgments

The Geochemistry Lab at the University of Modena and Reggio Emilia has been funded through a initial grant of the Programma Giovani Ricercatori Rita Levi Montalcini to AC. This project received funds by the European Research Council (ERC) under the European Union's Horizon 2020 Research and Innovation Programme (grant agreement No 724046 – SUCCESS awarded to SB) and the MIUR FARE programme 2018 (FARE Ricerca in Italia: Framework per l'attrazione e il rafforzamento delle eccellenze - SAPIENS project to SB). Mattia Sisti is thanked for initiating the collection of Sr isotope data and Silvia Cercatillo for water sampling. We thank Sonia García de Madinabeitia, José Ignacio Gil Ibarguchi and an anonymous reviewer for their constructive comments.

References

Adams, S., Grün, R., McGahan, D., Zhao, J., Feng, Y., Nguyen, A., Willmes, M., Quaresimin, M., Lobsey, B., Collard, M., 2019. A strontium isoscape of north-east Australia for human provenance and repatriation. Geoarchaeology 34, 231–251.

Argentino, C., Lugli, F., Cipriani, A., Panieri, G., 2021. Testing miniaturized extraction chromatography protocols for combined 87Sr/86Sr and ∂88/86Sr analyses of pore water by MC-ICP-MS. Limnol. Oceanogr. Methods 19, 431–440.

418 Bataille, C.P., Bowen, G.J., 2012. Mapping 87Sr/86Sr variations in bedrock and water for large scale provenance
419 studies. Chem. Geol. 304, 39–52.

420 Bataille, C.P., Von Holstein, I.C.C., Laffoon, J.E., Willmes, M., Liu, X.-M., Davies, G.R., 2018. A bioavailable
421 strontium isoscape for Western Europe: A machine learning approach. PLoS One 13, e0197386.

422 Bataille, C.P., Crowley, B.E., Wooller, M.J., Bowen, G.J., 2020. Advances in global bioavailable strontium
423 isoscapes. Palaeogeogr. Palaeoclimatol. Palaeoecol. 555, 109849.

424 Bataille, C.P., Jaouen, K., Milano, S., Trost, M., Steinbrenner, S., Crubézy, É., Colleter, R., 2021. Triple sulfur-
425 oxygen-strontium isotopes probabilistic geographic assignment of archaeological remains using a novel sulfur
426 isoscape of western Europe. PLoS One 16, e0250383.

427 Bentley, R.A., 2006. Strontium isotopes from the earth to the archaeological skeleton: A review. J. Archaeol.
428 Method Theory 13, 135–187.

429 Bowen, G.J., 2010. Isoscapes: spatial pattern in isotopic biogeochemistry. Annu. Rev. Earth Planet. Sci. 38, 161–
430 187.

431 Britton, K., Le Corre, M., Willmes, M., Moffat, I., Grün, R., Mannino, M.A., Woodward, S., Jaouen, K., 2020.
432 Sampling Plants and Malacofauna in 87Sr/86Sr Bioavailability Studies: implications for isoscape mapping and
433 reconstructing of past mobility patterns. Front. Ecol. Evol. 8, 579473.

434 Capo, R.C., Stewart, B.W., Chadwick, O.A., 1998. Strontium isotopes as tracers of ecosystem processes: theory
435 and methods. Geoderma 82, 197–225.

436 Cardarelli, A., Cavazzuti, C., Quondam, F., Salvadei, L., Salzani, L., 2015. Le necropoli delle Narde di Frattesina:
437 proposta per una lettura delle evidenze demografiche, rituali e sociali a partire dai dati archeologici e antropologici.
438 Le necropoli delle Narde di Frat. Propos. per una Lett. delle evidenze Demogr. Ritual. e Soc. a partire dai dati
439 Archeol. e Antropol. 437–445.

440 Cavazzuti, C., Cardarelli, A., Quondam, F., Salzani, L., Ferrante, M., Nisi, S., Millard, A.R., Skeates, R., 2019a.
441 Mobile elites at Frattesina: flows of people in a Late Bronze Age 'port of trade' in northern Italy. Antiquity 93,
442 624–644.

443 Cavazzuti, C., Skeates, R., Millard, A.R., Nowell, G., Peterkin, J., Brea, M.B., Cardarelli, A., Salzani, L., 2019b.
444 Flows of people in villages and large centres in Bronze Age Italy through strontium and oxygen isotopes. PLoS
445 One 14, e0209693.

446 Cavazzuti, C., Hajdu, T., Lugli, F., Sperduti, A., Vicze, M., Horváth, A., Major, I., Molnár, M., Palcsu, L., Kiss,
447 V., 2021. Human mobility in a Bronze Age Vatya 'urnfield' and the life history of a high-status woman. PLoS One
448 16, e0254360.

449 Chesson, L.A., Tipple, B.J., Ehleringer, J.R., Park, T., Bartelink, E.J., 2018. Forensic applications of isotope
450 landscapes ("isoscapes"): a tool for predicting region-of-origin in forensic anthropology cases. Forensic Anthropol.
451 Theor. Framew. Sci. basis 127–148.

452 Colleter, R., Bataille, C.P., Dabernat, H., Pichot, D., Hamon, P., Duchesne, S., Labaune-Jean, F., Jean, S., Le
453 Cloirec, G., Milano, S., 2021. The last battle of Anne of Brittany: solving mass grave through an interdisciplinary
454 approach (paleopathology, biological anthropology, history, multiple isotopes and radiocarbon dating). PLoS
455 One 16, e0248086.

456 Conrad, O., Bechtel, B., Bock, M., Dietrich, H., Fischer, E., Gerlitz, L., Wehberg, V., Wichmann, Böhner, J.
457 (2015). System for automated geoscientific analyses (SAGA) v. 2.1. 4. Geosci. Model Dev. 8, 1991-2007.

458 Copeland, S.R., Cawthra, H.C., Fisher, E.C., Lee-Thorp, J.A., Cowling, R.M., le Roux, P.J., Hodgkins, J.,
459 Marean, C.W., 2016. Strontium isotope investigation of ungulate movement patterns on the Pleistocene Paleo-
460 Agulhas Plain of the Greater Cape Floristic Region, South Africa. Quat. Sci. Rev. 141, 65–84.

461 Ehrlich, S., Gavrieli, I., Dor, L.-B., Halicz, L., 2001. Direct high-precision measurements of the 87 Sr/86 Sr isotope
462 ratio in natural water, carbonates and related materials by multiple collector inductively coupled plasma mass
463 spectrometry (MC-ICP-MS). J. Anal. At. Spectrom. 16, 1389–1392.

464 Emery, M. V, Stark, R.J., Murchie, T.J., Elford, S., Schwarcz, H.P., Prowse, T.L., 2018. Mapping the origins of
465 Imperial Roman workers (1st–4th century CE) at Vagnari, Southern Italy, using 87Sr/86Sr and d18O variability.
466 Am. J. Phys. Anthropol. 166, 837–850.

467 Erel, Y., Torrent, J., 2010. Contribution of Saharan dust to Mediterranean soils assessed by sequential extraction
468 and Pb and Sr isotopes. Chem. Geol. 275, 19–25.

469 Ericson, J., 1985. Strontium isotope characterization in the study of prehistoric human ecology. J. Hum. Evol. 14,
470 503–514.

471 Evans, J.A., Montgomery, J., Wildman, G., Boulton, N., 2010. Spatial variations in biosphere 87Sr/86Sr in
472 Britain. J. Geol. Soc. London. 167, 1–4.

473 Faure, G., Mensing, T.M., 2005. Isotopes: principles and applications, 3rd ed. John Wiley & Sons, Hoboken, New
474 Jersey.

475 Frank, A.B., Frei, R., Moutafi, I., Voutsaki, S., Orgeolet, R., Kristiansen, K., Frei, K.M., 2021. The geographic
476 distribution of bioavailable strontium isotopes in Greece–A base for provenance studies in archaeology. Sci. Total
477 Environ. 148156.

478 Frei, K.M., Frei, R., 2011. The geographic distribution of strontium isotopes in Danish surface waters - A base for
479 provenance studies in archaeology, hydrology and agriculture. Appl. Geochemistry 26, 326–340.

480 Funck, J., Bataille, C., Rasic, J., Wooller, M., 2021. A bio-available strontium isoscape for eastern Beringia: a tool
481 for tracking landscape use of Pleistocene megafauna. J. Quat. Sci. 36, 76–90.

482 Gregoricka, L.A., 2021. Moving Forward: A Bioarchaeology of Mobility and Migration. J. Archaeol. Res. doi:
483 10.1007/s10814-020-09155-9.

484 Han, G., Song, Z., Tang, Y., Wu, Q., Wang, Z., 2019. Ca and Sr isotope compositions of rainwater from Guiyang
485 city, Southwest China: Implication for the sources of atmospheric aerosols and their seasonal variations. Atmos.
486 Environ. 214, 116854.

487 Hartman, G., Richards, M., 2014. Mapping and defining sources of variability in bioavailable strontium isotope
488 ratios in the Eastern Mediterranean. Geochim. Cosmochim. Acta 126, 250–264.

489 Hedman, K.M., Slater, P.A., Fort, M.A., Emerson, T.E., Lambert, J.M., 2018. Expanding the strontium isoscape
490 for the American midcontinent: Identifying potential places of origin for Cahokian and Pre-Columbian migrants.
491 J. Archaeol. Sci. Reports 22, 202–213.

492 Hobson, K.A., Barnett-Johnson, R., Cerling, T., 2010. Using isoscapes to track animal migration, in: Isoscapes.
493 Springer, pp. 273–298.

494 Holt, E., Evans, J.A., Madgwick, R., 2021. Strontium (87Sr/86Sr) mapping: a critical review of methods and
495 approaches. Earth-Science Rev. 103593.

496 Hoogewerff, J.A., Reimann, C., Ueckermann, H., Frei, R., Frei, K.M., van Aswegen, T., Stirling, C., Reid, M.,
497 Clayton, A., Ladenberger, A., 2019. Bioavailable 87 Sr/ 86 Sr in European soils: A baseline for provenancing
498 studies. Sci. Total Environ. 672, 1033–1044.

499 Killick, D.J., Stephens, J.A., Fenn, T.R., 2020. Geological constraints on the use of lead isotopes for provenance
500 in archaeometallurgy. Archaeometry 62, 86–105.

501 Knudson, K.J., Williams, H.M., Buikstra, J.E., Tomczak, P.D., Gordon, G.W., Anbar, A.D., 2010. Introducing
502 δ88/86Sr analysis in archaeology: a demonstration of the utility of strontium isotope fractionation in paleodietary
503 studies. J. Archaeol. Sci. 37, 2352–2364.

504 Kootker, L.M., van Lanen, R.J., Kars, H., Davies, G.R., 2016. Strontium isoscapes in The Netherlands. Spatial
505 variations in 87Sr/86Sr as a proxy for palaeomobility. J. Archaeol. Sci. Reports 6, 1–13.

506 Krige, D.G., 1951. A statistical approach to some basic mine valuation problems on the Witwatersrand. J. South.
507 African Inst. Min. Metall. 52, 119–139.

508 Ladegaard-Pedersen, P., Achilleos, M., Dörflinger, G., Frei, R., Kristiansen, K., Frei, K.M., 2020. A strontium
509 isotope baseline of Cyprus. Assessing the use of soil leachates, plants, groundwater and surface water as proxies
510 for the local range of bioavailable strontium isotope composition. Sci. Total Environ. 708, 134714.

511 Laffoon, J.E., Sonnemann, T.F., Shafie, T., Hofman, C.L., Brandes, U., Davies, G.R., 2017. Investigating human
512 geographic origins using dual-isotope (87Sr/86Sr, δ18O) assignment approaches. PLoS One 12, e0172562.

513 Lazzerini, N., Balter, V., Coulon, A., Tacail, T., Marchina, C., Lemoine, M., Bayarkhuu, N., Turbat, T., Lepetz,
514 S., Zazzo, A., 2021. Monthly mobility inferred from isoscapes and laser ablation strontium isotope ratios in
515 caprine tooth enamel. Sci. Rep. 11, 1–11.

516 Lightfoot, E., O'Connell, T.C., 2016. On the use of biomineral oxygen isotope data to identify human migrants
517 in the archaeological record: intra-sample variation, statistical methods and geographical considerations. PLoS
518 One 11, e0153850.

519 Lugli, F., Cipriani, A., Peretto, C., Mazzucchelli, M., Brunelli, D., 2017. In situ high spatial resolution $^{87}Sr/^{86}Sr$
520 ratio determination of two Middle Pleistocene (c.a. 580 ka) *Stephanorhinus hundsheimensis* teeth by LA–MC–
521 ICP–MS. Int. J. Mass Spectrom. 412, 38–48.

522 Lugli, F., Cipriani, A., Tavaglione, V., Traversari, M., Benazzi, S., 2018. Transhumance pastoralism of
523 Roccapelago (Modena, Italy) early-modern individuals: Inferences from Sr isotopes of hair strands. Am. J. Phys.
524 Anthropol. 167, 470-483.

525 Lugli, F., Cipriani, A., Capecchi, G., Ricci, S., Boschin, F., Boscato, P., Iacumin, P., Badino, F., Mannino, M.A.,
526 Talamo, S., Richards, M.P., Benazzi, S., Ronchitelli, A., 2019. Strontium and stable isotope evidence of human
527 mobility strategies across the Last Glacial Maximum in southern Italy. Nat. Ecol. Evol. 3, 905–911.

528 Maurer, A., Galer, S.J.G., Knipper, C., Beierlein, L., Nunn, E. V, Peters, D., Tütken, T., Alt, K.W., Schöne, B.R.,
529 2012. Bioavailable 87Sr/86Sr in different environmental samples — Effects of anthropogenic contamination and
530 implications for isoscapes in past migration studies. Sci. Total Environ. 433, 216–229.

531 McArthur, J.M., Howarth, R.J., Bailey, T.R., 2001. Strontium isotope stratigraphy: LOWESS version 3: best fit
532 to the marine Sr-isotope curve for 0-509 Ma and accompanying look-up table for deriving numerical age. J. Geol.
533 109, 155–170.

534 Montgomery, J., Evans, J. a., Wildman, G., 2006. 87Sr/86Sr isotope composition of bottled British mineral waters
535 for environmental and forensic purposes. Appl. Geochemistry 21, 1626–1634.

536 Muhlfeld, C.C., Thorrold, S.R., McMahon, T.E., Marotz, B., 2012. Estimating westslope cutthroat trout
537 (*Oncorhynchus clarkii lewisi*) movements in a river network using strontium isoscapes. Can. J. Fish. Aquat. Sci.
538 69, 906–915.

539 Négrel, P., Guerrot, C., Millot, R., 2007. Chemical and strontium isotope characterization of rainwater in France:
540 influence of sources and hydrogeochemical implications. Isotopes Environ. Health Stud. 43, 179–196.

Oliver, M.A., Webster, R., 1990. Kriging: a method of interpolation for geographical information systems. Int. J. Geogr. Inf. Syst. 4, 313–332.

Pederzani, S., Britton, K., 2019. Oxygen isotopes in bioarchaeology: Principles and applications, challenges and opportunities. Earth-Science Rev. 188, 77–107.

Pellegrini, M., Pouncett, J., Jay, M., Pearson, M.P., Richards, M.P., 2016. Tooth enamel oxygen "isoscapes" show a high degree of human mobility in prehistoric Britain. Sci. Rep. 6, 34986.

Pestle, W.J., Simonetti, A., Curet, L.A., 2013. 87Sr/86Sr variability in Puerto Rico: geological complexity and the study of paleomobility. J. Archaeol. Sci. 40, 2561–2569.

Pors Nielsen, S., 2004. The biological role of strontium. Bone 35, 583–8.

Scaffidi, B.K., Knudson, K.J., 2020. An archaeological strontium isoscape for the prehistoric Andes: Understanding population mobility through a geostatistical meta-analysis of archaeological 87Sr/86Sr values from humans, animals, and artifacts. J. Archaeol. Sci. 117, 105121.

Sillen, A., Hall, G., Richardson, S., Armstrong, R., 1998. 87Sr/86Sr ratios in modern and fossil food-webs of the Sterkfontein Valley: implications for early hominid habitat preference. Geochim. Cosmochim. Acta 62, 2463–2473.

Slovak, N.M., Paytan, A., 2012. Applications of Sr Isotopes in Archaeology, in: Baskaran, M. (Ed.), Handbook of Environmental Isotope Geochemistry. Springer, pp. 743–768.

Smith, K.E., Weis, D., Amini, M., Shiel, A.E., Lai, V.W.-M., Gordon, K., 2019. Honey as a biomonitor for a changing world. Nat. Sustain. 2, 223–232.

Snoeck, C., Ryan, S., Pouncett, J., Pellegrini, M., Claeys, P., Wainwright, A.N., Mattielli, N., Lee-Thorp, J.A., Schulting, R.J., 2020. Towards a biologically available strontium isotope baseline for Ireland. Sci. Total Environ. 712, 136248.

Song, B.-Y., Ryu, J.-S., Shin, H.S., Lee, K.-S., 2014. Determination of the source of bioavailable Sr using 87Sr/86Sr tracers: a case study of hot pepper and rice. J. Agric. Food Chem. 62, 9232–9238.

565 Soto, D.X., Wassenaar, L.I., Hobson, K.A., 2013. Stable hydrogen and oxygen isotopes in aquatic food webs are
566 tracers of diet and provenance. Funct. Ecol. 27, 535–543.

567 Thomsen, E., Andreasen, R., 2019. Agricultural lime disturbs natural strontium isotope variations: Implications
568 for provenance and migration studies. Sci. Adv. 5, eaav8083.

569 Tommasini, S., Marchionni, S., Tescione, I., Casalini, M., Braschi, E., Avanzinelli, R., Conticelli, S., 2018.
570 Strontium isotopes in biological material: A key tool for the geographic traceability of foods and humans beings,
571 in: Behaviour of Strontium in Plants and the Environment. Springer, pp. 145–166.

572 Toncala, A., Trautmann, B., Velte, M., Kropf, E., Mcglynn, G., 2020. On the premises of mixing models to define
573 local bioavailable 87Sr / 86Sr ranges in archaeological contexts. Sci. Total Environ. 745, 140902.

574 Vautour, G., Poirier, A., Widory, D., 2015. Tracking mobility using human hair: What can we learn from lead
575 and strontium isotopes? Sci. Justice 55, 63–71.

576 Voerkelius, S., Lorenz, G.D., Rummel, S., Quétel, C.R., Heiss, G., Baxter, M., Brach-Papa, C., Deters-Itzelsberger,
577 P., Hoelzl, S., Hoogewerff, J., Ponzevera, E., Van Bocxstaele, M., Ueckermann, H., 2010. Strontium isotopic
578 signatures of natural mineral waters, the reference to a simple geological map and its potential for authentication
579 of food. Food Chem. 118, 933–940.

580 Wang, X., Tang, Z., 2020. The first large-scale bioavailable Sr isotope map of China and its implication for
581 provenance studies. Earth-Science Rev. 103353.

582 Washburn, E., Nesbitt, J., Ibarra, B., Fehren-Schmitz, L., Oelze, V.M., 2021. A strontium isoscape for the
583 Conchucos region of highland Peru and its application to Andean archaeology. PLoS One 16, e0248209.

584 Weber, M., Tacail, T., Lugli, F., Clauss, M., Weber, K., Leichliter, J., Winkler, D.E., Mertz-Kraus, R., Tütken, T.,
585 2020. Strontium uptake and intra-population 87Sr/86Sr variability of bones and teeth—controlled feeding
586 experiments with rodents (Rattus norvegicus, Cavia porcellus). Front. Ecol. Evol. 8, 569940.

587 Willmes, M., Bataille, C.P., James, H.F., Moffat, I., McMorrow, L., Kinsley, L., Armstrong, R.A., Eggins, S.,
588 Grün, R., 2018. Mapping of bioavailable strontium isotope ratios in France for archaeological provenance studies.
589 Appl. Geochemistry 90, 75–86.

590 Yanes, Y., Delgado, A., Castillo, C., Alonso, M.R., Ibáñez, M., De la Nuez, J., Kowalewski, M., 2008. Stable
591 isotope (δ18O, δ13C, and δD) signatures of recent terrestrial communities from a low-latitude, oceanic setting:
592 endemic land snails, plants, rain, and carbonate sediments from the eastern Canary Islands. Chem. Geol. 249,
593 377–392.

594 Zieliński, M., Dopieralska, J., Królikowska-Ciągło, S., Walczak, A., Belka, Z., 2021. Mapping of spatial variations
595 in Sr isotope signatures (87Sr/86Sr) in Poland—Implications of anthropogenic Sr contamination for
596 archaeological provenance and migration research. Sci. Total Environ. 775, 145792.

597